



Continuous Fluorescence Depletion Anisotropy Measurement of Protein Rotation

Dongmei Zhang¹ · Jinming Song¹ · Jason Pace¹ · Deborah A. Roess² · B. George Barisas¹

Received: 25 November 2017 / Accepted: 22 January 2018 / Published online: 3 February 2018
© Springer Science+Business Media, LLC, part of Springer Nature 2018

Abstract

Protein rotation in viscous environments can be measured by fluorescence depletion anisotropy (FDA) which combines long lifetimes of chromophore triplet states with the sensitivity of fluorescence excitation and detection. FDA achieves sensitivity well beyond that attainable by the more common technique of time-resolved phosphorescence anisotropy (TPA). We have now combined benefits of both time-domain and frequency-domain FDA into a single continuous technique (CFDA). Intensity and polarization of a single laser beam are modulated continuously according to a complex, repeating waveform. Fluorescence signals excited from triplet-forming fluorescent probes are digitized over recurring waveform periods by a high-speed signal averager. CFDA experiments typically involve substantial ground state depletion. Thus signals, unlike those of TPA, are not linear in the exciting light intensity and simple data analysis based on such linearity is not appropriate. An exact solution of the coupled diffusion and triplet production/decay equation describing CFDA within individual data points has been combined with simulated annealing optimization to extract triplet and anisotropy decay kinetics from experimental data. Related calculations compare possible excitation waveforms with respect to rotational information provided per fluorescence photon. We present CFDA results for the model system of eosin conjugates of carbonic anhydrase, BSA and immunoglobulin G in 90% glycerol at various temperatures and initial cellular results on eosin-IgE bound to 2H3 cell Type I Fcε receptors. We explore how CFDA reflects rotational parameters of heterogeneous systems and discuss challenges of extending this method to single cell microscopic measurements.

Keywords Eosin · Diffusion · Phosphorescence · Triplet

Introduction

Changes in the motions of integral membrane proteins reflect and/or modulate primary events in cellular activation [1, 2]. In particular, rates of rotational diffusion [3] reflect protein interactions, aggregation and conformation and so are sensitive measures of the size and microenvironment of these molecules. Experimentally, unhindered rotational diffusion occurs on the microsecond timescale and has been studied using various methods, including linear dichroism, delayed fluorescence, time-resolved phosphorescence anisotropy (TPA) and fluorescence depletion anisotropy (FDA) [4–6].

However, cellular studies demand robust, broadly-applicable methods and only the latter two of these methods have been widely used.

The anisotropy function describes the orientational asymmetry of any molecular distribution and is in fact the simplest quantitative measure of the deviation of the emission dipole distribution from spherical symmetry. Emission anisotropy r is calculated as $(I_{\parallel} - I_{\perp}) / (I_{\parallel} + 2I_{\perp})$ where I_{\parallel} and I_{\perp} are luminescence intensities polarized parallel and perpendicular, respectively, to the polarization of an exciting pulse. The anisotropy of a freely-rotating *spherical* species in solution decays mono-exponentially with a rotational correlation time τ of $1/6D = \eta V_h / kT$ where D is the rotational diffusion constant, η is the viscosity and V_h is the molecular hydrated volume. Chromophores in the asymmetric environment of a membrane can exhibit multiple rotational correlation times plus a non-decaying component or “limiting” anisotropy. However, distinct rotational correlation times can rarely be resolved in practice, so it is most common to represent apparent decay as

✉ B. George Barisas
george.barisas@colostate.edu

¹ Department of Chemistry, Colorado State University, Fort Collins, CO 80523, USA

² Department of Biomedical Sciences, Colorado State University, Fort Collins, CO 80523, USA

$r = r_{\infty} + (r_0 - r_{\infty}) \exp(-t/\varphi)$ where φ is an average rotational correlation time. This quantity clearly reflects size, asymmetry, environment and interactions of the rotating molecule.

Protein rotation in viscous solutions or on cell surfaces can be measured by various methods. Time-resolved phosphorescence anisotropy (TPA) measurements of protein rotation are analogous to the better-known time-resolved fluorescence anisotropy (TFA) methods. However, singlet lifetimes of fluorescent probes are typically only a few nanoseconds, hence TFA is limited to measuring low-nanosecond time-scale rotations. Apart from low quantum yields of suitable phosphors, the necessarily long triplet state lifetimes imply low photon fluxes, even at saturation, and long-wavelength phosphorescence is poorly detected by most high-speed detectors. By contrast, fluorophores typically exhibit high quantum yields, nanosecond lifetimes and mid-visible fluorescence emission.

It is thus natural to ask if the long lifetime of triplet states could be combined with the sensitivity of fluorescence excitation and detection. Such a technique, Fluorescence Depletion Anisotropy, was proposed by Peter Garland [7] and used subsequently by our group in a number of studies [8–10]. The method depends upon fluorophores like eosin isothiocyanate (EITC) which have substantial quantum yields both for triplet formation and for prompt fluorescence [11]. Rotationally mobile macromolecules labeled with such a chromophore are first irradiated by a low-intensity, linearly-polarized probe beam (Fig. 1 upper panel), e.g. from an Ar-ion laser at

514.5 nm. The resulting steady-state fluorescence is proportional to the number of ground state chromophores whose absorption transition dipoles are parallel to the probe polarization. The sample is then subjected to a brief pulse of high-intensity, linearly polarized light. A pulsed Nd:YAG laser producing mJ pulses at 532 nm is appropriate to examine 1 mm² of sample. Under this intense illumination, a substantial fraction of chromophores undergo intersystem crossing to the triplet state. These triplets can exist for several hundred microseconds and, during this period, they cannot be excited to fluoresce by the probe beam. Thus, immediately after the pump pulse, there is asymmetric depletion in sample fluorescence which recovers back to the original steady state by the mechanisms of triplet decay and rotational reorientation. By recording traces in the presence and absence of both pump and probe beams, undesired signals from sample autofluorescence, gating transients, etc. are cancelled automatically.

The relative advantage of FDA over TPA can be estimated by considering the major photophysical processes in a three-level system (Fig. 2). The maximum FDA fluorescence signal reflecting the non-fluorescent, slowly-decaying triplet state can be compared with the maximum phosphorescence signal arising from this or from another chosen chromophore. If one ignores reverse intersystem crossing k_R , the maximum fluorescence rate arising in FDA from triplet decay is approximately $\Phi_f \Phi_i / \tau_t$ where, for the FDA chromophore, Φ_f and Φ_i are the quantum yields for prompt fluorescence and inter-system crossing, respectively, and τ_t is the triplet lifetime. The maximum phosphorescence rate in TPA is approximately one phosphorescence quantum yield Φ_p of photons per phosphorescence lifetime τ_p or Φ_p / τ_p . The relative signal advantage of FDA over TPA is thus $(\Phi_f \Phi_i / \Phi_p) (\tau_p / \tau_t)$. Comparing eosin in FDA with erythrosin in TPA, this advantage is 10- to 100-fold. This sensitivity enhancement relative to TPA has allowed protein rotation measurements via FDA on individually-selected cells [12]. Nonetheless there are practical difficulties in time-domain FDA measurements. Apart from the photophysical limitations on signal intensities just described, there are instrumental

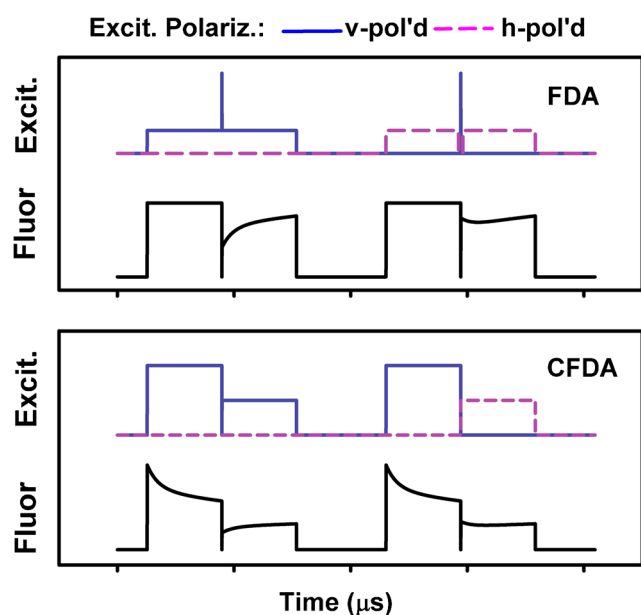


Fig. 1 Rotation information in pulse fluorescence depletion anisotropy (FDA) and continuous fluorescence depletion anisotropy (CFDA) data. Blue (solid) lines and red (dashed) lines in upper panel halves marked “lasers” indicate vertical and horizontal polarizations, respectively

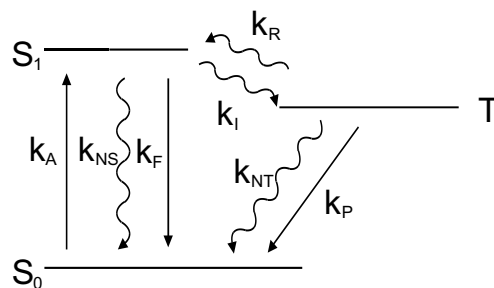


Fig. 2 Jablonski diagram showing major photophysical processes in a three-level system

constraints on data acquisition rate, detector saturation from excitation pulse and waste of fluorescence photons during excitation pulse.

While the above limitations might be approached by improved dyes, faster lasers combined with fast photon counting and more effective detector gating, frequency domain measurements may also appear to address at least the latter two issues. We have previously investigated frequency-domain FDA where a continuous-wave laser's intensity and polarization are modulated by frequencies ν and w , respectively [13]. Unfortunately, intrinsic non-linearity of FDA spreads rotation information into many frequencies, e.g. ν , w , 2ν , $2w$, $\nu-w$, $\nu+w$, 2ν , $2w$, $2(\nu-w)$, $2(\nu+w)$, $2\nu-w$, etc. Thus efficient collection of distributed rotational information actually amounts to performing a time-domain experiment.

One may wonder if advantages of time- and frequency-domain approaches could be combined into single technique. Intensity and polarization of a single laser beam would be modulated continuously according to a complex, repetitive waveform and fluorescence signals averaged over recurring waveform periods by a low rearm-time signal averager. This would offer prospective advantages of no gating, no wasted fluorescence, use of a single laser and data collection in a continuous experiment. We have previously realized such a technique, continuous fluorescence depletion anisotropy (CFDA), and described preliminary experiments measurements using the approach [14]. In the present paper we describe an improved approach to analysis of resulting data and present rotational information obtained on glycerol solutions of well-known proteins at various temperatures as well as initial cellular results on eosin-IgE bound to 2H3 cell Type I Fcε receptors. Our goal in this project is to evaluate the suitability of CFDA for further development aimed at measuring protein rotation on cell surfaces.

Theory Underlying Data Analysis

Consider an L-format optical system with excitation along the z-axis and emission acquired along the x-axis. Samples consist of freely-rotating macromolecules to which chromophores are rigidly attached. The absorption and fluorescence emission transition dipoles are assumed here to be collinear, a reasonable approximation for the xanthine dyes such as fluorescein and eosin. However, a similar treatment can be developed for non-collinear transition dipoles. On the timescale of experiments and at light intensities employed, chromophores can be assumed to exist only in the singlet ground state and the first triplet excited state.

The rate constant for triplet formation by light of unit intensity polarized parallel to the absorption transmission dipole is given by

$$k_b = \frac{3.2303 \epsilon_M \Phi_T h c}{\lambda N_A} \quad (1)$$

where ϵ_M is the molar absorptivity, Φ_T is the triplet quantum yield, h is Planck's constant, c is the speed of light, N_A is Avogadro's number and λ is the wavelength. The factor of 3 arises since ϵ_M is defined for randomly-oriented molecules.

The basic equation for CFDA is expressed in terms of the distribution function $c(\theta, \phi, t)$ of ground state chromophore transition dipoles

$$k_r \nabla^2 c(\theta, \phi, t) + k_d(1 - c(\theta, \phi, t)) - k_b I(\theta, \phi, t) c(\theta, \phi, t) = \frac{\partial c(\theta, \phi, t)}{\partial t}, \quad (2)$$

where k_r is the rotational diffusion constant of the chromophore, k_d is the decay rate of triplet chromophores to the ground-state, k_b is the rate of excitation of ground-state chromophores to the triplet state and $I(\theta, \phi, t)$ is the intensity of time- and polarization-varying exciting light on the sample.

Since $\nabla^2 Y_n^m(\theta, \phi) = -n(n+1)Y_n^m(\theta, \phi)$, we can express c as a sum of even-order spherical harmonics $Y_n^m(\theta, \phi)$

$$c(\theta, \phi, t) = \sum_{n=0}^{\infty} \sum_{m=-n}^{step\ 2\ n\ step\ 2} a_n^m(t) Y_n^m(\theta, \phi) \quad (3)$$

Without loss of generality, we can assume that $c(\theta, \phi, 0) = 1/\sqrt{4\pi}$ so that $a_0^0(0) = 1$. For a given set of k_d , k_r and k_b , combining Eqs. (2) and (3) yields

$$\frac{\partial a_n^m(t)}{\partial t} - k_d = n(n+1)k_r a_n^m(t) - k_d a_n^m(t) - k_b I(\theta, \phi, t) a_n^m(t) \quad (4)$$

Sample illumination $I(\theta, \phi, t)$ affects Y_n^m in the right-hand side of Eq. (4). Our illumination consists of mixtures of x- and y-polarized light of intensities $I_x(t)$ and $I_y(t)$, respectively, so that $I_x(t) = \sin^2 \theta \cos^2 \phi I_{x0}(t)$ and $I_y(t) = \sin^2 \theta \sin^2 \phi I_{y0}(t)$. Interaction of such light with a given Y_n^m produces up to 9 spherical harmonics ranging from Y_{n-2}^{m-2} up to Y_{n+2}^{m+2} . Explicit equations for the magnitudes of these new Y_n^m can be derived from the properties of spherical harmonics or their underlying associated Legendre polynomials [15]. The distribution function c can be obtained as a power series in $k_b I$. If n is the order of a given term in that series, then the term will be comprised of spherical harmonics up to order $2n$. Such a series converges unconditionally and we have explored this approach. However, convergence is slow when k_d and/or k_r are large and an alternate solution is desirable.

The indices n and m of a spherical harmonic Y_n^m uniquely determine its position i in a list where all Y_n^m are ordered, first, by increasing n and, then, by increasing m , as shown in Eq. (5). Hence all spherical harmonics can be described as members of a one-dimensional array with index i . Simple

relations allow i to be evaluated from n and m and, conversely, n and m from i . Hence we can consider c to be a function of a fixed number of even spherical harmonics up to some order n_{\max} . Then the distribution function c will consist of $(n_{\max}/2 + 1)^2$ terms. As a concrete example, if n_{\max} is 2, there are four terms. For simplification, let $I_{s_0}(t) = I_{x_0}(t) + I_{y_0}(t)$ and $I_{d_0}(t) = I_{x_0}(t) - I_{y_0}(t)$.

light of unit intensity can be decomposed into four spherical harmonics.

$$\begin{aligned} x^2 &= \sqrt{4\pi} [Y_0^0 - \sqrt{3/10} Y_2^0 + \sqrt{1/5} (Y_2^2 + Y_2^{-2})]; \\ y^2 &= \sqrt{4\pi} \left[Y_0^0 - \sqrt{3/10} Y_2^0 - \sqrt{1/5} (Y_2^2 + Y_2^{-2}) \right] \end{aligned} \tag{8}$$

$$\begin{aligned} &\begin{vmatrix} \frac{1}{3} k_b I_{s_0}(t) & \frac{1}{\sqrt{30}} k_b I_{d_0}(t) & \frac{-1}{3\sqrt{5}} k_b I_{s_0}(t) & \frac{1}{\sqrt{30}} k_b I_{d_0}(t) \\ \frac{1}{\sqrt{30}} k_b I_{s_0}(t) & \frac{3}{7} k_b I_d(t) + k_d + 6k_r & \frac{-1}{7} \sqrt{\frac{2}{3}} k_b I_{s_0}(t) & 0 \\ \frac{-1}{3\sqrt{5}} k_b I_{s_0}(t) & \frac{-1}{7} \sqrt{\frac{2}{3}} k_b I_{d_0}(t) & \frac{5}{21} k_b I_{s_0}(t) + k_d + 6k_r & \frac{-1}{7} \sqrt{\frac{2}{3}} k_b I_{d_0}(t) \\ \frac{1}{\sqrt{30}} k_b I_{s_0}(t) & 0 & \frac{-1}{7} \sqrt{\frac{2}{3}} k_b I_{s_0}(t) & \frac{3}{7} k_b I_{s_0}(t) + k_d + 6k_r \end{vmatrix} \begin{vmatrix} a_0^0(t) \\ a_2^{-2}(t) \\ a_2^0(t) \\ a_2^2(t) \end{vmatrix} - \begin{vmatrix} a_0^0(0) \\ a_2^{-2}(0) \\ a_2^0(0) \\ a_2^2(0) \end{vmatrix} = \begin{vmatrix} k_d \\ 0 \\ 0 \\ 0 \end{vmatrix} \\ &\text{or} \\ &\mathbf{B}(t)\mathbf{A}(t) - \mathbf{A}(0) = |k_d, 0, 0 \dots|^T \equiv \mathbf{f}(t) \end{aligned} \tag{5}$$

Thus an inhomogeneous equation of the form shown can be used to describe the chromophore distribution function to whatever precision desired.

Fluorescence elicited by light of either polarization is calculated using the orthonormality of spherical harmonics. The choice for leading constants is such that initial fluorescence from unit excitation intensity is 1. Our experimental configuration uses a magic-angle polarizer to measure total emitted fluorescence [17] so that, if E is the efficiency of fluorescence collection, the measured total fluorescence F is

As written, this system of inhomogeneous linear first-order differential equations has non-constant coefficients $I_{x_0}(t)$, $I_{y_0}(t)$ and, as such, is only soluble with substantial difficulty. A satisfactory alternate approach is to consider the equation pointwise. Since the exciting laser intensity remains constant during each measurement point, the equation may readily be solved at each point using as initial conditions the results of the previous point. The entire experimental signal can thus be generated for specified rate constants and other parameters as desired. Solution of Eq. (5) at a given point follows standard procedures [16]. For the matrix \mathbf{B} in the left-hand side of Eq. (5), eigenvalues λ_i are calculated as a vector of length n and corresponding eigenvectors as an $n \times n$ matrix $\mathbf{\Lambda}$, respectively. An n -vector $\lambda(t)$ whose elements λ_i are $\exp(\lambda_i t)$ is generated and a matrix $\mathbf{M}(t)$ is constructed as $\mathbf{M}(t) = \mathbf{\Lambda} \text{Diag}[\lambda(t)]$. The solution $\mathbf{A}(t)$ of the inhomogeneous equation at time t following an initial value $\mathbf{A}(t_0)$ is then given by

$$\begin{aligned} F &= E [I_{x_0}(t) + I_{y_0}(t)] a_0^0(t) - \sqrt{1/5} [I_{x_0}(t) + I_{y_0}(t)] a_2^0(t) \\ &+ \sqrt{1/5} [I_{x_0}(t) - I_{y_0}(t)] [a_2^2(t) + a_2^{-2}(t)] \end{aligned} \tag{9}$$

We assume that triplet decay and molecular rotation are independent of each other. Then triplet decay is characterized by n_d multiple decay rates k_{di} , with fractions f_{dj} and molecular rotation is specified by n_r multiple rotational decay rates or correlation times k_{rj} with fractions f_{rj} and the overall signal $F_o(t)$ becomes

$$\mathbf{A}(t) = \mathbf{M}(t)\mathbf{M}^{-1}(t_0)\mathbf{A}(t_0) + \mathbf{M}(t) \int_{t_0}^t \mathbf{M}^{-1}(s) \mathbf{f}(s) ds \tag{6}$$

The time-dependent orientational distribution function $c(\theta, \varphi, t)$ can thus be evaluated as

$$F_o(t) = \sum_{i=1}^{n_d} \sum_{j=1}^{n_r} f_i f_j F(k_{di}, k_{rj}, t) \tag{10}$$

$$c(\theta, \varphi, t) = \mathbf{A}(t) \cdot \left| Y_0^0(\theta, \varphi), Y_2^{-2}(\theta, \varphi), Y_2^0(\theta, \varphi), Y_2^2(\theta, \varphi) \dots \right|^T \tag{7}$$

to any desired precision by incorporating spherical harmonics up to a sufficiently large order n .

Data analysis according to Eq. 10 involves considerable computation, the amount of which increases strongly with the number of constants fitted. We therefore fitted CFDA data to seven fixed lifetimes, typically 8, 24, 80, 240, 800, 2400 and 8000 μs , evaluating the best-fitting decay fraction of each lifetime. The rotational behavior of the macromolecule is modeled assuming a limiting anisotropy r_∞ representing rotationally-immobile species and amplitude $(r_0 - r_\infty)$ decaying as a single exponential, i.e. with a single rotational correlation time. We can evaluate the rotation fractional amplitudes f_{rj} for 3 rotation rates, the first k_{r1} being arbitrarily fast and representing sub-microsecond

motions, the second k_{r2} representing overall protein rotation and the third k_{r3} being zero and so representing the rotationally-immobile fraction of chromophores. To maintain consistency with TPA and TFA experiments, we can then report $(f_{r2} + f_{r3})$ as the “initial anisotropy” r_0 , $1/6k_{r2}$ as the protein RCT and f_{r3} as the “limiting anisotropy” r_∞ .

Even if the decay rates k_{di} are considered fixed, the preceding treatment nonetheless specifies a large number of independent parameters which must be adjusted to optimize agreement between the observed and calculated fluorescence traces. We initially employed the Marquardt non-linear fitting procedure [18] but found that searches became trapped in local minima. Even when small random increments were added to parameters to restart trapped searches, global minima were not reached.

Satisfactory optimizations were achieved using the so-called Simulated Annealing method of Goffe et al. [19]. This procedure simulates the process by which melted substances, through slow cooling, escape from defect traps to reach a minimum-energy crystalline state. Briefly, a system is assigned a starting “temperature” and initial parameter set. A random variation in parameters is introduced and a system “energy”, here the average square deviation between observed and calculated fluorescence, is evaluated. If the parameter change reduces the energy, i.e. improves the fit, then that parameter change is accepted and a new parameter change attempted. However, if the energy is increased by the parameter change, i.e. $\Delta E > 0$, then that change may be rejected *or* accepted. The quantity $\exp(-\Delta E/aT)$ where a is a constant is compared to a random number between 0 and 1 and the parameter change accepted if the random number is smaller. Thus, parameter changes that only slightly increase energy are most likely to be accepted, but changes substantially increasing energy nonetheless have finite probabilities of acceptance. As the search proceeds, the temperature and the parameter step sizes are reduced to simulate the annealing process.

Experimental Methods

Apparatus and Data Acquisition

The apparatus used in CFDA experiments is shown in Fig. 3 and has been described in a preliminary report [14]. Continuous wave excitation at 514.5 nm is provided by the vertically-polarized TEM00 output from a Coherent Radiation Innova 90 argon ion laser. A Lasermetrics 3031 transverse Pockels cell (Lasermetrics Inc./FastPulse Technology, Teaneck, NJ), driven by a Lasermetrics AF-3 driver, rotates the beam polarization in response to a waveform generated in timing hardware, the response time being less than 200 ns for a 90° rotation. The beam intensity is

then adjusted by a Coherent 304 acoustic-optic modulator (AOM; Coherent Inc., Modulator Division, Danbury, CT) in response to an input waveform. Maximum modulated power at the sample is approximately 100 mW. To increase laser intensity at the sample, a 2x Galilean telescope reduces the beam $1/e^2$ diameter to approximately 0.7 mm. A Tektronix AF320 Arbitrary Function Generator generates waveforms for the Pockels cell and AOM. A half-wave plate set at 22° adjusts the polarization of the un-rotated and rotated beams to +45° and –45° with respect to the vertical. Samples are examined in 5 × 5 mm Suprasil cuvetts (Helma). Sample fluorescence is collected at 90° to the excitation axis and through a polarizer set at 35° to the vertical. Fluorescence of any polarization is thus collected with equal efficiency [17] so that the measured signal is proportional to the total emitted fluorescence. Depletion data thus reflect *only* the orientation of *absorption* transition dipoles and, as such, are true absorption anisotropies. Scattered light and phosphorescence are removed by a $K_2Cr_2O_7$ chemical filter, a Schott KV550 filter and a 600 nm short-pass interference filter and fluorescence is detected using an EMI9816 photomultiplier tube (PMT; Thorn EMI Gencom Inc., Plainview, NY). PMT signals are amplified by a Tektronix 473 oscilloscope and averaged by an EG&G 9826 signal average with 0.6 μs re-arm time. In a typical experiment 256 k points, 256 ns/pt, are digitized per trace and 4096 traces are averaged at a repetition rate of 16 traces/sec.

Test systems exhibiting rotational correlation times comparable to many membrane proteins were prepared from 200 to 500 nM solutions of eosin isothiocyanate-conjugated proteins [20] in approximately 90% glycerol and examined over 4–37 °C, with actual glycerol concentrations in samples determined by measurement of refractive index. Bovine IgG, bovine serum albumin (BSA) and bovine carbonic anhydrase (CA) were obtained from Sigma Chemical Co. (St. Louis, MO).

Independent measurements of eosin triplet, i.e. phosphorescence, lifetime were performed using an IBH 5000U fluorescence lifetime spectrometer equipped with xenon flash lamp and multichannel scaling for phosphorescence lifetime measurements. Excitation was at 526 nm and emission was recorded at 680 nm. Band widths were 16 nm and 32 nm, respectively. Data from ~ 110,000 lamp flashes were acquired in 1000 0.5 μs channels and were analyzed beginning at 5 μs after the lamp flash to avoid including the large fluorescence transient immediately after each flash. Decay was fitted to a single exponential decay model.

Waveform Selection

Any light waveform where intensity changes both with and without polarization change can yield rotation information and many such optical waveforms are possible. Waveform

Fig. 3 Apparatus for Continuous Fluorescence Depletion Anisotropy (CFDA) measurements on bulk samples. The functions of the various components are described in the text

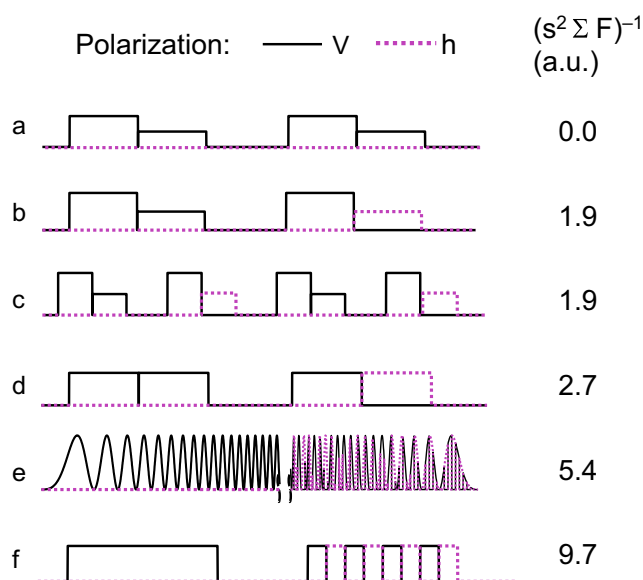
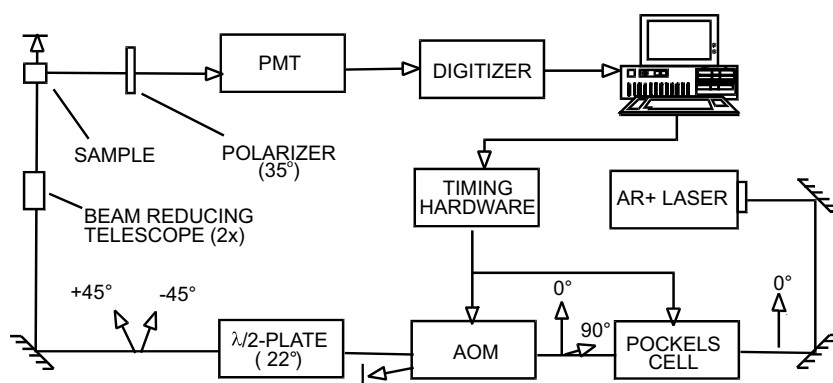


Fig. 4 Relative efficiencies of various waveform types in using available fluorescence photons in evaluating the rotational correlation time of a rotating species in solution. All traces represent 4096 points with triplet decay times of 3, 30 & 300 points and fractional amplitudes of 0.3, 0.4 & 0.3 respectively. Rotational correlation time is 30 points in all cases

optimization must be with respect to a specific parameter for a typical sample. A suitable figure of merit for optimization is $(s^2 \Sigma F)^{-1}$, the reciprocal of the squared standard error for a particular parameter multiplied by the total intensity in the detected waveform from which the parameter is estimated. This quantity increases as the desired parameter is better defined from a constant amount of sample fluorescence.

We calculated this figure of merit for accuracy of determining rotational correlation time for the waveforms illustrated in Fig. 4. The upper waveform (a) where the polarization never changes contains no rotational information. The next two waveforms (b, c) where four shorter sections in the latter replace two longer ones but with equal total power, exhibit equal figures of merit. Waveform (d) with four equal intensity segments, one of which

involves a polarization change, affords substantially more information. The chirp waveform (e), where intensity changes over the range of triplet decay times both with and without polarization change over the range of rotational correlation times, is even more efficient. The most efficient waveform is (f). Acousto-optic modulators exhibit substantial nonlinearity, so it is difficult to determine the exact optical intensity provided by a given electrical waveform. However, the uniform-intensity waveform (f) provides even more information than the chirp, while avoiding calibration issues. Hence we currently use a single illuminated intensity to avoid issues of AOM non-linearity.

Data Obtained

Figure 5 shows a complete example waveform used to generate rotation data. The illuminated portions of the waveform were separated by substantial dark intervals. This was done to guarantee complete decay of light-induced triplet states between illuminated sections, thus possibly simplifying analysis. However, we emphasize that this is not necessary as our analysis scheme applies to *any* repetitive waveform. Hence, shortening the dark intervals shown in Fig. 5 would increase the rate of data acquisition by several-fold.

Rotation information is available whenever the polarization of the exciting light is changed. This phenomenon is most clearly in Fig. 6 where the sum of Fig. 5 sections B and D is subtracted from the sum of sections A and C. This removes the large fluorescence decrease over time resulting from the exciting light conversion of chromophores to triplets. The actual dependence of fluorescence signal on the intensity and polarization of the exciting light is exceptionally complex as shown in the “[Theory Underlying Data Analysis](#)” section and inclusion of this complexity is essential in quantitative analysis of CFDA data.

Data analysis involves optimizing agreement between the full 4-section fluorescence trace such as shown in Fig. 5 and points calculated from Eq. 10. The standard deviation of

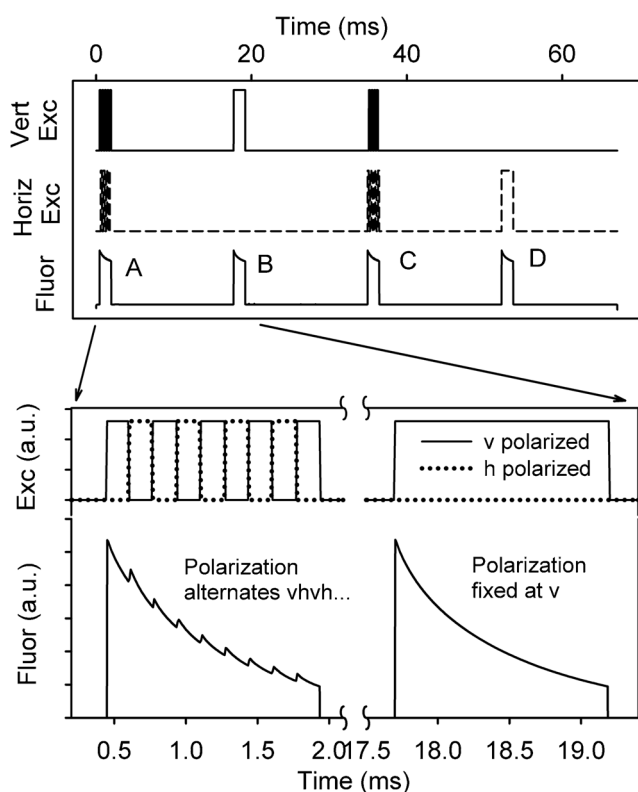


Fig. 5 Excitation waveform and raw fluorescence data for CFDA measurement of EITC-BSA rotation at 4 °C in 90% glycerol

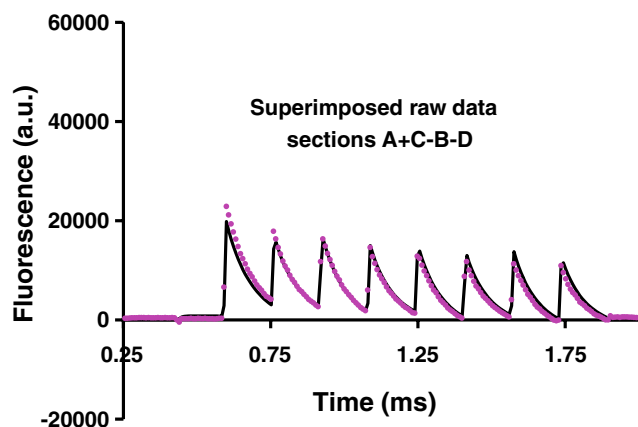


Fig. 6 Excitation waveform and raw fluorescence data for CFDA measurement of EITC-BSA rotation at 4 °C in 90% glycerol. Dotted lines indicate raw data while the smooth line represents fitted curves calculated by Eq. (10)

experimental points about best-fitted curves for full-scale fluorescence signals of over 1×10^6 is typically 500–1000, a relative standard error less than 0.1%. The quality of such agreement can be visualized by examination of Fig. 6.

Results and Discussion

Protein Rotation vs. Temp, Viscosity

We examined by CFDA the rotation of three proteins, IgG, BSA and CA, in ~90% glycerol over 4–37 °C. Table 1 shows the rotational correlation times τ of eosin-conjugates of these proteins. Because neither the hydrated partial specific volume \bar{V}_h nor the effective axial ratio p of the proteins under these conditions is known, the expected values of the rotational correlation time cannot be predicted precisely. What can be said is that the rotational correlation time τ of a freely-rotating protein is given by

$$\tau = f \bar{V}_h \eta M / RT = f (\bar{V}_p + \delta \bar{V}_w) \eta M / RT \quad (11)$$

where \bar{V}_h , \bar{V}_p and \bar{V}_w are the partial specific volumes of the hydrated protein, the protein alone and its bound water, respectively, δ is the amount of bound water and f is a factor reflecting asymmetry of the hydrated particle [21]. Hence, a plot of τ vs. $\eta M / RT$ should have a slope of $f \bar{V}_h$ which should be approximately constant for a given protein in solutions of fixed composition. In fact, Fig. 7 shows the RCT of each protein to vary linearly with $\eta M / RT$ and the slopes of such plots are indicated beside the best-fit lines and range from 1.9 to 2.9. Moreover, when the RCTs and corresponding $\eta M / RT$ for the three proteins are plotted on log–log plots, the slopes are 0.9–1.0, as predicted by Eq. 11. While the uncertainties in RCT values are clearly substantial, increasing the waveform duty cycle and/or increasing the laser intensity at the sample should allow very substantial improvement.

Protein rotation in water has been examined by other investigators and their measured RCTs can be compared with our results. For carbonic anhydrase at room temperature, values of 14.6 ns [22] and 11.2 ns [23] have been reported. Immunoglobulin decay is strongly multi-exponential on account of the segmental flexibility of the Fab domains but, for the slow component reflecting overall molecular rotation, the mean of several studies [23–26] is approximately 130 ns. Several investigators have examined BSA, but a particularly careful examination by Ferrer et al. [27] using several methods gives a mean value of 40 ± 2 ns at 20 °C (1.00 cP).

Information concerning rotation of proteins in glycerol solutions is more limited. Using NMR methods Korchuganov [28] finds that addition of 20% glycerol almost doubles the RCT of barnase at 31.5 °C from 5.51 ns (0.77cP) to 9.38 ns (1.79 cP). For BSA in 95% glycerol at 23 °C Yao et al. [29] obtain a value of 22 μ s while, for BSA in 92% glycerol at 6 °C, Ferrer et al. [27] report 47 μ s. The RCTs of barnase and BSA both increase linearly with η/T as expected. In general, Prieu et al. [30] suggest that glycerol causes compaction of the protein core but increases the size of the hydration layer.

Table 1 CFDA measurements of protein rotation in 90% glycerol solutions

| Sample | Temp | RCT (μs) ^a | r_0^b | r_∞^b | $t_{1/2}$ (CFDA, μs) | $t_{1/2}$ (from TPA lifetime, μs) |
|--------|------|------------------------------------|---------|--------------|----------------------------------|---|
| IgG | 4 | 146.4 \pm 12.6 | 0.096 | 0.000 | 160 | – |
| IgG | 15 | 46.8 \pm 8.2 | 0.224 | 0.009 | 167 | – |
| IgG | 25 | 16.3 \pm 7.9 | 0.235 | 0.006 | 103 | – |
| IgG | 37 | 7.8 \pm 2.3 | 0.324 | 0.013 | 23 | – |
| Bsa | 4 | 101.3 \pm 11.4 | 0.238 | 0.000 | 280 | 177 |
| Bsa | 15 | 38.1 \pm 1.7 | 0.282 | 0.001 | 169 | 157 |
| Bsa | 25 | 20.4 \pm 2.0 | 0.267 | 0.004 | 171 | 142 |
| Bsa | 37 | 8.4 \pm 2.3 | 0.313 | 0.012 | 99 | 122 |
| Ca | 4 | 29.6 \pm 8.2 | 0.190 | 0.004 | 140 | – |
| Ca | 15 | 13.8 \pm 1.4 | 0.163 | 0.003 | 114 | – |
| Ca | 25 | 10.6 \pm 3.9 | 0.259 | 0.003 | 186 | – |
| Ca | 37 | 6.9 \pm 4.1 | 0.220 | 0.006 | 150 | – |

^aIndicated uncertainties are the estimated standard deviations of the averaged RCTs

^bUncertainties in these quantities are discussed in the text

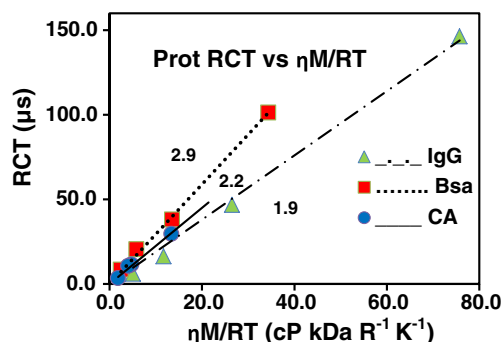


Fig. 7 RCT of IgG, BSA and carbonic anhydrase in ~90% glycerol as functions of solution temperature and viscosity. Estimated uncertainties for points are given in Table 1. Slopes of the fitted lines are shown beside each plot

Typical values for \bar{V}_p and δ in water are $0.73 \text{ cm}^3 \text{ g}^{-1}$ and $0.40 \text{ g H}_2\text{O per g protein}$ [21], so that \bar{V}_h might be estimated at $1.13 \text{ cm}^3 \text{ g}^{-1}$. If proteins are modeled as rotation ellipsoids, effects of asymmetry can be predicted from protein axial ratios p calculated from ultracentrifuge data or intrinsic viscosity measurements. For fluorescence anisotropy, Perrin's treatment [31] predicts three rotational correlation times for ellipsoids of revolution. In practice, for axial ratios of about 5 or less, the actual decay curve cannot be distinguished from a single exponential. Axial ratios reported for IgG, BSA and CA in water at room temperature are 5.4 [32], 3.5 [33] and 5.4 [34], respectively. Thus, for an axial ratio of 3.5, relative to an equal-volume sphere, the RCTs and (fractional amplitudes) are predicted to be 0.97 (0.4), 1.92 (0.4) and 2.84 (0.2). Such a decay can be characterized by the harmonic mean of the rotational correlation times [31] or as the single exponential which can be best-fitted to the theoretical three-exponential

decay. On the latter basis, for axial ratios of 3.5 and 5.4, single RCTs of 1.73 and 2.44, respectively, times those of equivalent spheres would be predicted. These quantities can be multiplied by \bar{V}_h to predict slopes of plots of RCT vs $\eta\text{M}/\text{RT}$ for the various proteins. For IgG, BSA and CA, predicted slopes are 2.8, 2.0 and 2.8 while experimental slopes, shown on Fig. 7, are 1.9, 2.9 and 2.2, respectively. Taken together, these estimates of \bar{V}_h and f can largely explain the observation that RCTs of globular proteins are typically 2–3 times theoretical values [35] and that the slopes of plots of RCT vs $\eta\text{M}/\text{RT}$ in Fig. 7 fall in this range.

Initial and Limiting Anisotropy Values

Samples examined by CFDA exhibit initial anisotropies averaging 0.23 ± 0.06 while limiting anisotropies are 0.004 ± 0.007 . The first quantity is a typical absorption anisotropy for a chromophore conjugated to a protein [36], since nanosecond- timescale flexibility substantially reduces the initial anisotropy from its theoretical value of 2/5. Limiting anisotropies for solutions of homogeneous macromolecules should be zero, so the standard deviation of measured anisotropies perhaps indicates the uncertainty in absolute anisotropies measured by these methods.

Lifetime Values and Distributions

To accommodate the multi-exponential triplet decay observed in CFDA, we have fitted this decay to a set of seven fixed lifetimes, typically 8, 24, 80, 240, 800, 2400 and 8000 μs . Examples of resulting decay distributions for EITC-BSA at 4 °C and 37 °C are shown in Fig. 8. At 4 °C,

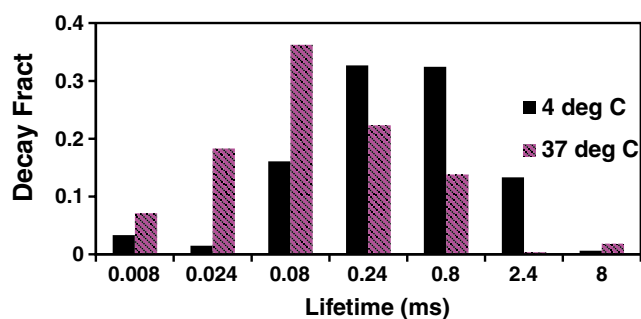


Fig. 8 Triplet decay distributions for EITC-BSA in 90% glycerol at 4° and 37°C

the peak decay amplitudes are at 240 and 800 μ s while, at 37 °C, peak decays are at 80 and 240 μ s. How such distributions relate to that lifetime(s) observed in a technique like time-resolved phosphorescence anisotropy (TPA) is complex. This is because, in TPA, an initial distribution of triplet chromophores is produced by a high-intensity and asymmetric pulse of nominally negligible width and this distribution decays by only by triplet decay and rotational randomization. In CFDA, the evolution of fluorescence over time also involves continuous pumping of molecules into the triplet state throughout the experiment by exciting light. This situation is properly modeled by Eq. 10 but precisely how the resulting lifetime distributions such as those shown in Fig. 8 relate to what might be observed in a TPA measurement is not clear. One possible comparison is to use the complete CFDA lifetime distributions to calculate apparent decay half-times $t_{1/2}$ and compare these quantities with 0.69 times the triplet lifetimes measured directly by TPA. Half-times ranging from approximately 100–300 μ sec as evaluated by these two methods are shown in Table 1 and are in reasonable agreement, given the differences in the methods being compared.

Preliminary Cellular Results

The apparatus described in this paper was intended for measurements on cuvet-sized samples of protein solutions. However, suspended 2H3 cells labeled with EITC-A2-IgE were also examined at 4 °C using single-intensity waveforms, albeit with small fluorescence signals and high noise (Fig. 9). The fitted RCT is approximately 76 μ s and this can be compared with a value of 82 ± 17 μ s obtained for erythrosin isothiocyanate-labeled A2-IgE in extensive TPA studies [37]. The CFDA method should be much more promising if implemented in a microscope-based system. The key factor in such expected improvement would be the much smaller illuminated area and resulting

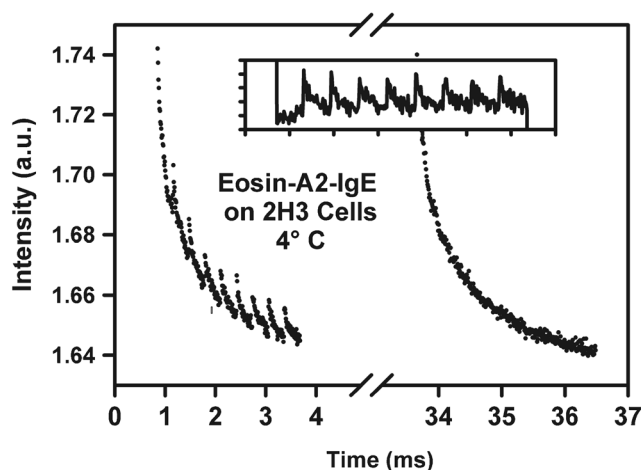


Fig. 9 CFDA examination of suspended 2H3 mucosal mast cells at 4 °C binding eosin isothiocyanate-conjugated A2 IgE. The fitted RCT is 76 μ s. The inset shows the difference between fluorescence excited by light of alternating polarization and that from fixed polarization. See Fig. 5

more intense illumination at the sample. For example, cuvet samples are examined in a Gaussian beam of diameter 0.7 mm. In a microscope implementation intended for examination of individual cells, the illuminated diameter might be 20 μ m. For a given laser intensity, the peak intensity on a microscope sample would be about 800-fold greater than on a cell in the cuvet and hence a 20–50 mW frequency-doubled Nd:YAG laser would provide almost ideal illumination.

Conclusions

Fluorescence Depletion Anisotropy (FDA) combines the long lifetime of triplet states with the sensitivity of fluorescence excitation and detection to allow measurement of protein rotation in solution or on cell surfaces. Combination of time- and frequency-domain FDA in a single technique, Continuous Fluorescence Depletion Anisotropy (CFDA), provides protein rotation measurements via a continuous, single-laser method with no gating and no wasted photons. Rotational correlation times measured for common proteins in glycerol solutions exhibit the expected dependence on solution viscosity and temperature. Moreover the technique appears to have unique potential for measuring rotation of specific proteins on individual living cells, as will be examined in future studies.

Acknowledgements The Authors are grateful to Professor Israel Pecht of the Weizmann Institute of Science, Rehovot, Israel, for his kind gift of the A2 IgE used in the preliminary cellular studies.

References

- Axelrod D (1983) Lateral motion of membrane proteins and biological functions. *J Membr Biol* 75:1–10
- Edidin M (1974) Rotational and translational diffusion in membranes. *Annu Rev Biophys Bioeng* 3:179–201
- Hoffmann W, Sarzala MG, Chapman D (1979) Rotational motion and evidence for oligomeric structures of sarcoplasmic reticulum Ca-activated ATPase. *Proc Natl Acad Sci USA* 3860–3864
- Cherry RJ (1978) Measurement of protein rotational diffusion in membranes by flash photolysis. *Methods Enzymol* 54:47–61
- Cherry R (1979) Rotational and lateral diffusion of membrane proteins. *Biochem Biophys Acta* 559:289–327
- Greinhart R, Stark H, Steir A, Weller A (1979) E-type delayed fluorescence depletion, a technique to probe rotational correlation time in the microsecond range. *J Biochem Biophys Methods* 1:77–83
- Johnson P, Garland PB (1981) Depolarization of fluorescence depletion. A microscopic method for measuring rotational diffusion of membrane proteins on the surface of a single cell. *FEBS Lett* 132(2):252–256
- Barisas BG, Rahman NA, Yoshida TM, Roess DA (1990) Rotation of plasma membrane proteins measured by polarized fluorescence depletion. *Proc SPIE* 1204:765–774
- Yoshida TM, Zarrin F, Barisas BG (1988) Measurement of protein rotational motion using frequency domain polarized fluorescence depletion. *Biophys J* 54:277–288
- Yoshida TM, Barisas BG (1986) Protein rotational motion in solution measured by polarized fluorescence depletion. *Biophys J* 50(1):41–53
- Garland PB, Moore CH (1979) Phosphorescence of protein-bound eosin and erythrosin. A possible probe for measurements of slow rotational mobility. *Biom J* 183:561–572
- Barisas BG, Roess DA, Pecht I, Rahman NA (1990) Rotational dynamics of Fc_ε receptors on individual 2H3 RBL cells studied by polarized fluorescence depletion. *Biophys J* 75:671
- Yoshida TM (1989) Measurement of protein rotational diffusion using time-and frequency-domain polarized fluorescence depletion. Thesis, Colorado State University
- Barisas BG, Zhang H (2001) Continuous fluorescence depletion anisotropy (CFDA) measurement of protein rotation. *Proc SPIE* 4260:140–148
- Jackson JD (1962) Mathematics for quantum mechanics: an introductory survey of operators, eigenvalues, and linear vector spaces, 1st edn. W.A. Benjamin, Inc., New York
- Kaplan W (1958) Ordinary differential equations
- Wegener WA, Rigler R (1984) Separation of translational and rotational contributions in solution studies using fluorescence photobleaching recovery. *Biophys J* 46:787–793
- Marquardt DW (1963) An algorithm for least-squares estimation of nonlinear parameters. *J Soc Ind Appl Math* 11(2):431–441
- Goffe WL, Ferrier GD, Rogers J (1994) Global optimization of statistical functions with simulated annealing. *J Econ* 60:65–99
- Rahman NA, Pecht I, Roess DA, Barisas BG (1992) Rotational dynamics of type I Fc epsilon receptors on individually-selected rat mast cells studied by polarized fluorescence depletion. *Biophys J* 61(2):334–346
- Cantor CR, Schimmel PR (1980) Biophysical chemistry part II: techniques for the study of biological structure and function. W.H. Freeman and Company, San Francisco, p 441
- Kask P, Piksarv P, Mets U, Pooga M, Lippmaa E (1987) Fluorescence correlation spectroscopy in the nanosecond time range: rotational diffusion of bovine carbonic anhydrase B. *Eur Biophys J* 14:257–261
- Yguerabide J, Epstein HF, Stryer L (1970) Segmental flexibility in an antibody molecule. *J Mol Biol* 51(3):573–590
- Riddiford CL, Jennings BR (1967) Kerr effect study of the aqueous solutions of three globular proteins. *Biopolymers* 5:557–571
- Lovejoy C, Holowka DA, Cathou RE (1977) Nanosecond fluorescence spectroscopy of pyrenebutyrate-anti-pyrene antibody complexes. *Biochemistry* 16(16):3668–3672
- Chan LM, Cathou RE (1977) The role of the inter-heavy chain disulfide bond in modulating the flexibility of immunoglobulin G antibody. *J Mol Biol* 112(4):653–656
- Ferrer ML, Duchowicz R, Carrasco B, de la Torre JG, Acuna AU (2001) The conformation of serum albumin in solution: a combined phosphorescence depolarization-hydrodynamic modeling study. *Biophys J* 80(5):2422–2430
- Korchuganov DS, Gagnidze IE, Tkach EN, Schulga AA, Kirpichnikov MP, Arseniev AS (2004) Determination of protein rotational correlation time from NMR relaxation data at various solvent viscosities. *J Biomol NMR* 30(4):431–442
- Yao J, McStay D, Rogers AJ, Quinn PJ (1992) A comparative study of rotational relaxations of an eosin-protein complex using delayed fluorescence and phosphorescence. *J Mod Opt* 39(11):2363–2373
- Priev A, Almagor A, Yedgar S, Gavish B (1996) Glycerol decreases the volume and compressibility of protein interior. *Biochemistry* 35(7):2061–2066
- perrin F (1936) Mouvement brownien d'un ellipsoïde (II). Rotation libre et depolarisation des fluorescences. Translation et diffusion de molecules ellipsoïdales. *J Phys Radium* 7(1):1–11
- Monkos K, Turczynski B (1991) Determination of the axial-ratio of globular-proteins in aqueous-solution using viscometric measurements. *Int J Biol Macromol* 13(6):341–344
- Squire PG, Moser P, O'Konski CT (1968) The hydrodynamic properties of bovine serum albumin monomer and dimer. *Biochemistry* 7(12):4261–4272
- McCoy LF, Wong KP (1981) Renaturation of bovine erythrocyte carbonic anhydrase-B denatured by acid, heat, and detergent. *Biochemistry* 20(11):3062–3067
- Tilley L, Sawyer WH, Morrison JR, Fidge NH (1988) Rotational diffusion of human lipoproteins and their receptors as determined by time-resolved phosphorescence anisotropy. *J Biol Chem* 263(33):17541–17547
- Londo TR, Rahman NA, Roess DA, Barisas BG (1993) Fluorescence depletion measurements in various experimental geometries provide true emission and absorption anisotropies for the study of protein rotation. *Biophys Chem* 48(2):241–257
- Song J, Hagen GM, Roess DA, Pecht I, Barisas BG (2002) The mast cell function-associated antigen and its interactions with the type I Fc epsilon receptor. *Biochemistry* 41(3):881–889